AIAA SciTech Forum
11–15 & 19–21 January 2021, VIRTUAL EVENT
AIAA Scitech 2021 Forum

10.2514/6.2021-0868

Enhanced Power Generation of Airborne Wind Energy System by a Foldable Aircraft

Myungjin Jung [*], Qiji Ze [†]
The Ohio State University, Columbus, Ohio, 43210

Chaoying Pei [‡]
Purdue University, Indiana, IN, 47907

Changhuang Wan [§], Kai Chuen Tan [¶], Ruike Zhao [‖]
The Ohio State University, Columbus, Ohio, 43210

Ran Dai [**]
Purdue University, Indiana, IN, 47907

This paper introduces a novel approach to improve the energy efficiency of a Ground-Gen airborne wind energy system (AWES) by changing the airborne platform's configuration. This research presents modeling and trajectory optimization approaches of an airborne platform during energy generation and recovery phases to improve net energy gain throughout a cycle. We first develop the flight dynamics of an AWES based on a conventional glider, as well as its power generation and consumption models, where the ground component is a motor/generator system that portrays a DC machine's electric performance. An optimal control problem is then formulated to search for an optimal trajectory to maximize energy harvesting during the generation phase and minimum energy consumption during the recovery phase. In the end, the improvement of net energy gain and time reduction of the recovery phase by morphing the wing shape during the recovery phase is justified by comparing the simulation results between the folded wing model and the one using conventional glider geometry.

Nomenclature

Φ	=	the bank angle of a glider, rad
α	=	the angle of attack, rad
α_{w}	=	the angular acceleration of a winch, rad/s^2
γ	=	the flight path angle, rad
θ	=	the azimuth angle in spherical coordinate system, rad
ρ	=	the density of atmosphere, kg/m^3
ϕ	=	the zenith angle in spherical coordinate system, rad
ψ	=	the heading angle of a glider, rad
C_{D_f}	=	the aerodynamic drag coefficient of a folded wing glider
C_{D_g}	=	the aerodynamic drag coefficient of the glider in the generation phase
C_{D_u}	=	the aerodynamic drag coefficient of a folded wing glider
C_{L_f}	=	the aerodynamic lift coefficient of a folded wing glider
C_{L_g}	=	the aerodynamic lift coefficient of the glider in the generation phase
C_{L_u}	=	the aerodynamic lift coefficient of a unfolded wing glider

*Graduate Research Assistant, Mechanical and Aerospace Engineering Department. jung.661@osu.edu
†Postdoctoral Research Fellow , Mechanical and Aerospace Engineering Department. ze.3@osu.edu
‡Graduate Research Assistant, School of Aeronautics and Astronautics. peic@purdue.edu
§Graduate Research Assistant, Mechanical and Aerospace Engineering Department. wan.326@osu.edu
¶Former Undergraduate Research Assistant, Mechanical and Aerospace Engineering Department. tan.783@osu.edu
‖Assistant Professor, Mechanical and Aerospace Engineering Department. zhao.2885@osu.edu
**Associate Professor, School of Aeronautics and Astronautics. Senior Member AIAA. randai@purdue.edu

D	=	the aerodynamic drag force, N
F_t	=	the traction force, N
I_{w}	=	the moment of inertia of a winch, kg·m^2
L	=	the aerodyanmic lift force, N
M_{c}	=	the coulomb friction moment, N·m
M_{gen}	=	the torque of a generator, N·m
S_f	=	the wing area of a folded glider, m^2
S_u	=	the wing area of an unfolded glider, m^2
T	=	the thrust of a glider, N
W	=	the weight of a glider, N
m	=	the mass of a glider, kg
r	=	the distance between a glider and a DC machine
r_{w}	=	the radius of a winch, m
$\mathbf{V}_a$	=	the velocity of the glider in inertial coordinate system, m/s
$\mathbf{V}_e$	=	the effective wind velocity to the glider, m/s
$\mathbf{V}_l$	=	the velocity of the wind, m/s

I. Introduction

Wind energy is getting attraction as one of the most prominent renewable energy that has achieved 540 GW cumulative installed power worldwide by the end of 2017 and keeps increasing an extra 50 GW every year [1]. A significant number of efforts have focused on constructing taller towers for conventional ground-based wind turbines to take advantage of higher speed and steadier wind at a high altitude. Due to its higher construction cost and environmental constraints, power generation efficiency and flexibility have been significantly limited. To overcome such limitations of conventional wind turbines, the airborne wind energy system (AWES) was proposed in the 1980s with the capability of harvesting wind energy at significantly increased altitudes around 300 m - 5 km, which increases the average wind speed from 10 m/s to 30 m/s [2].

The Ground-Gen AWES, one of the most common mechanisms of AWESs, converts mechanical energy into electrical energy by pulling the tethered wire connected to the ground. This mechanism has attracted increasing attention from both research institutes and industries due to its low-cost for construction, high mobility, and easy operation. One energy production cycle of the Ground-Gen AWES is composed of a generation phase and a recovery phase. In the generation phase, traction force from an airborne platform tethered to the generator rotated by the tether line, that makes the generator's rotational motion, produces energy. In the recovery phase, on the other hand, the generator changes its role to a motor to rewind the tether and pull the airborne platform to the starting location for the next generation phase [3, 4]. Thus far, a great deal of research has been conducted for developing attitude control or trajectories during the generation phase, which usually accounts for 60% of the entire production cycle[5–9]. However, in the remaining 40% of the time period, extra energy and time consumption are required, which will reduce the net energy gain and efficiency of the power generation phase. Therefore, novel approaches are required to overcome current challenges in increasing the efficiency of AWES.

During the recovery phase, most external forces applied to the airborne platform are aerodynamic forces that impede the rewinding motion. Unlike a fixed-wing glider, morphing shape during the recovery phase provides adjusted aerodynamic characteristics that will shorten the period's length and reduce the power consumption. Unlike a kite, a fixed-wing aircraft has a propulsion system to provide additional thrust force when it is needed. In order to change the attitude of a kite, traction control [10] is used to change its bank angle or angle of attack. In addition, works in [11, 12] model the kite as a soft and inflatable body on the spherical coordinate system. Moreover, multi-body dynamics have been considered in [13, 14]. These approaches focus on the fluid-structure interaction that requires highly sophisticated modeling techniques. On the other hand, the glider platform has been selected for AWES because of extensive studies of rigid-wing aircraft and relatively simpler models compared to soft and flexible bodies, such as kites. Work in [15, 16] demonstrates the AWES based on the unmanned aerial vehicle (UAV) system derived from Lagrangian and [17] presents the six degree-of-freedom (DoF) UAV model based on principles of flight dynamics. Moreover, the thrust gives more flexibility to change the aircraft's attitude or velocity which contributes to the reduced duration and power consumption.

Several control strategies have been developed for AWES, e.g., figure-eight trajectory control [9]. Moreover, model predictive control has been applied to both generation and recovery phases [18]. However, there are limited studies on optimal control of the recovery phase. This paper aims to develop an optimal control scheme for a morphing airborne platform to reduce wind resistance leading to reduced time occupation and energy consumption of the recovery phase and eventually enhances energy generation efficiency.

The organization of this paper is as follows. §II introduces a foldable glider type Ground-Gen AWES and objective. §III demonstrates the entire AWES, including the glider, winch, and generator/motor. §IV presents the formulation of a multi-phase optimal control problem and the trajectory optimization approach. In §V, the integrated model for simulation is presented with results compared to a conventional glider model. Conclusions are addressed in §VI.

II. A Foldable Ground-Gen AWES

There are two major types of AWES. One is Ground-gen, where the generator is located on the surface of the ground. The generator produces electrical energy by pulling the line connected to the airborne platform. The other one is Fly-gen, where the airborne unit carries the generator and the energy is transmitted through the line to the ground station. In this study, we focused on a glider type Ground-Gen AWES. Compared to a kite, a Ground-Gen AWES has similar flight characteristics. Flying a kite on the ground has some physical limitations that impede continuous energy generation, such as the length of the line or wind speed. Therefore, one cycle of Ground-Gen AWES consists of two phases, the generation (traction) phase and the recovery (retrieval) phase. As shown in Fig. 1, a glider is connected to the ground DC machine with a line. During the generation phase, the glider keeps pulling the line with a particular flight pattern to reach a terminal condition. Then, we need to retrieve the released line such that the glider can be prepared for the next generation phase. In the recovery phase, the glider flies back to the initial position to restart the next cycle.

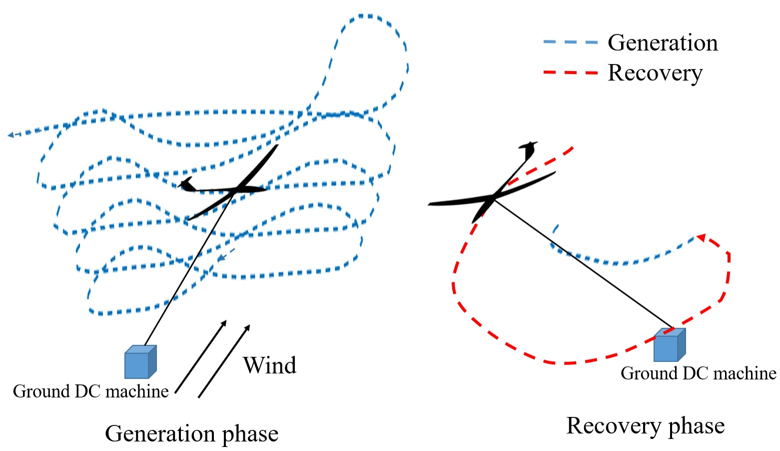

Fig. 1 Generation phase and recovery phase in glider type Ground-Gen AWES

Most Ground-Gen AWES studies have been conducted using kites to harvest wind energy. However, kites need extra energy to drive a motor to retrieve cable during the recovery phase. Kites are considered to have advantages in terms of wind energy harvesting since the effective area is generally larger than conventional wing type AWES. Larger effective area guarantees larger aerodynamic forces, which implies significantly increased traction force. However, a kite has limited maneuverability compared to a conventional aircraft. Thus, two issues in the recovery phase have been identified: 1) it takes a considerably long time to take the kite back, and 2) the system requires extra energy that can be dramatically increased in headwind scenarios. In order to address these issues, a glider type AWES is considered as an alternative option to reduce the time and energy consumption during the recovery phase.

In this paper, we propose the concept of a foldable wing configuration to retrieve the glider with much reduced time and energy consumption efficiently. As shown in Fig. 2, a glider with a foldable configuration folds to half of the wingspan. The glider will then require less energy to counteract the aerodynamic force due to the reduced wing area. Meanwhile, the folded wing configuration has a higher descent rate than the original configuration, leading to a reduced recovery duration. This study aims to verify the concept that a glider type AWES with foldable configuration can reduce time and energy consumption, which will eventually increase the efficiency of each energy harvesting cycle. For the generation and recovery phases, the glider has different physical characteristics and interaction modes with the DC machine. As shown in Fig. 3, the glider and DC machine's behavior will change according to the phase. In the next section, we will present the kinematic and dynamic models for the generation and recovery phase, respectively.

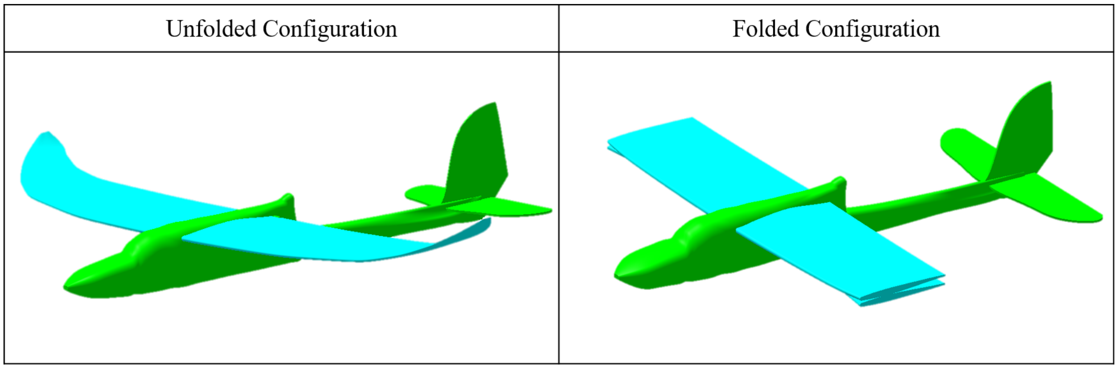

Fig. 2 Two configurations of a glider

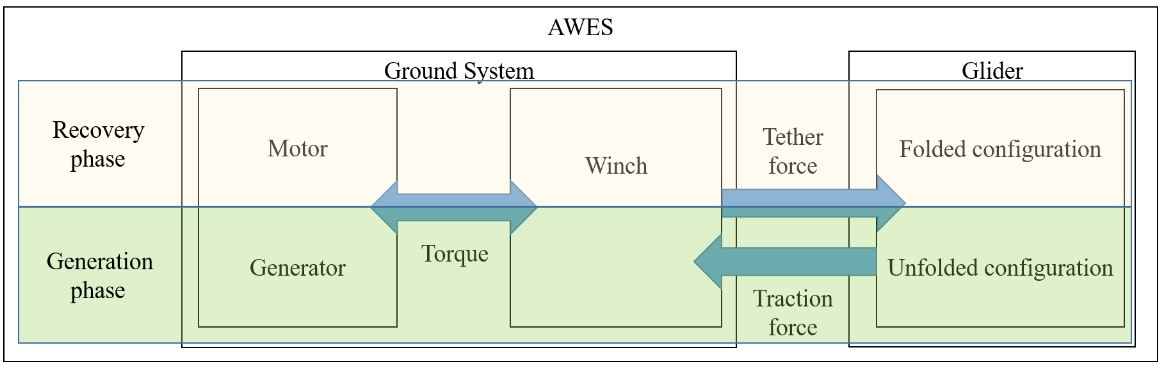

Fig. 3 The overview of the AWES model

III. AWES Model

In this section, the glider's kinematics and flight dynamics, as well as the dynamics of a ground system, are presented. For the generation phase, we use the spherical coordinate to facilitate the calculation of the traction force from the glider. In the recovery phase, we use the Cartesian coordinates to represent the dynamics of a glider. In addition, using characteristics of ground segments, we consider the transformation from mechanical energy into electrical energy.

A. Glider in Generation Phase

Assuming that the AWES generates wind energy near the surface, we can consider a flat Earth as a reference coordinate $\boldsymbol{E}$. $\boldsymbol{E}$ is defined with the X axis aligned with east, the Y axis aligned with north, and the Z axis pointing up from the surface. We also assume that the wind velocity direction is aligned with the X axis. Then the wind velocity vector is expressed as

$$\mathbf{V}_l = \begin{bmatrix} V_{wx} \\ 0 \\ 0 \end{bmatrix} \tag{1}$$

where V_{wx} is the component along the X axis, which is defined as

$$V_{wx} = 6 + 0.007z \tag{2}$$

In the spherical coordinate system, the position of the glider can be described by the distance between the glider and the ground station, denoted as r, zenith angle θ, and azimuth angle ϕ, shown in Fig 4a. The equations of motion of the glider are represented by

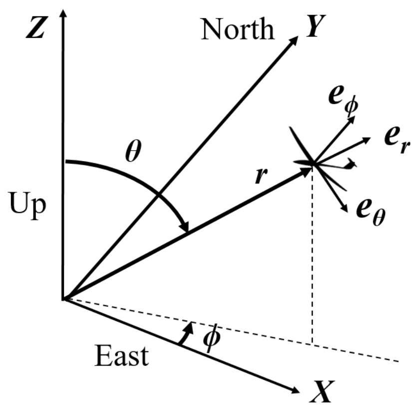

(a) Spherical / local coordinates

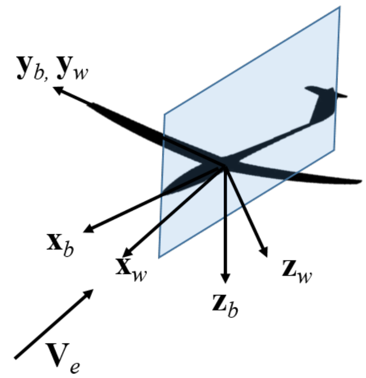

(b) Wind coordinate system of glider

Fig. 4 Coordinate systems of glider in generation phase

$$
\begin{aligned}
\frac{F_\theta}{m} &= r\ddot{\theta} - r\dot{\phi}^2 \sin\theta\cos\theta + 2\dot{\theta}\dot{r} \\
\frac{F_\phi}{m} &= r\ddot{\phi}\sin\theta + 2r\dot{\theta}\dot{\phi}\cos\theta + 2\dot{\theta}\dot{\phi}\sin\theta \\
\frac{F_r}{m} &= \ddot{r} - r\dot{\theta}^2 - r\dot{\phi}^2\sin^2\theta
\end{aligned}
\tag{3}
$$

where F_θ, F_ϕ, and F_r are the sum of the external force represented in the local coordinate system. The transformation of the two coordinates can be expressed as

$$
C_{ES} = \begin{bmatrix} \cos\theta\cos\phi & -\sin\phi & \sin\theta\cos\phi \\ \cos\theta\sin\phi & \cos\phi & \sin\theta\sin\phi \\ -\sin\theta & 0 & \cos\theta \end{bmatrix}
\tag{4}
$$

Then, the glider's position in the Cartesian coordinate is expressed as

$$
\begin{aligned}
x &= r\sin\theta\cos\phi \\
y &= r\sin\theta\sin\phi \\
z &= r\cos\theta
\end{aligned}
\tag{5}
$$

The external forces applied to the glider are aerodynamic forces, gravitational force, and traction force. In this study, the line's weight can be negligible because the scale of the airborne platform is smaller than commercial vehicles, and the distance is also relatively shorter. In addition, for the generation phase, we assume that the glider has a fixed angle of attack that has fixed aerodynamic coefficients C_{L_g}, C_{D_g} during the generation phase.

1. Aerodynamic Force

Aerodynamic forces can be determined by calculating the effective wind velocity $\mathbf{V_e}$, determined from

$$
\mathbf{V_e} = \mathbf{V_l} - \mathbf{V_a}
\tag{6}
$$

where $\mathbf{V}_a$ is the ground velocity, expressed in the local coordinate system as

$$
\mathbf{V}_a = \begin{bmatrix} \dot{\theta}r \\ \dot{\phi}r\sin\theta \\ \dot{r} \end{bmatrix}
\tag{7}
$$

Then, the magnitude of the effective wind speed can be calculated as below

$$\|\mathbf{V}_e\| = \|\mathbf{V}_l - C_{ES}\mathbf{V}_a\| \tag{8}$$

The aerodynamic forces can be derived in the local coordinate system, expressed as

$$\mathbf{F^a} = \begin{bmatrix} F_\theta^a \\ F_\phi^a \\ F_r^a \end{bmatrix} = -\frac{1}{2}\rho \|\mathbf{V_e}\|^2 S_u C_{L_g} \mathbf{z_w} - \frac{1}{2}\rho \|\mathbf{V_e}\|^2 S_u C_{D_g} \mathbf{x_w} \tag{9}$$

where ρ is the density of the air, S_u is the wing area of the glider, C_{L_g} and C_{D_g} are the lift and drag coefficient of the glider, and $\mathbf{x}_w$ and $\mathbf{z}_w$ are the basis vectors of the glider wind coordinate system, demonstrated in Fig 4b.

2. Gravitational Force

Due to the small scale of this AWES system that we proposed, the weight of the line between the ground station and glider can be neglected. The gravity force is directed along the -Z direction in the Cartesian coordinate. So we can derive the gravitational force in the local coordinate

$$\mathbf{F}^g = \begin{bmatrix} F_\theta^g \\ F_\phi^g \\ F_r^g \end{bmatrix} = C_{SE} \begin{bmatrix} 0 \\ 0 \\ -mg \end{bmatrix} = \begin{bmatrix} mg\sin\theta \\ 0 \\ -mg\cos\theta \end{bmatrix} \tag{10}$$

where m is the mass of the glider and g is the gravitational acceleration.

3. Traction Force

The traction force is applied to the kite along the e_r direction. By using the third equation in (3) and the external forces that we derived above, the traction force F^t is expressed as

$$\begin{aligned} F^t &= -F_r + F_r^g + F_r^a \\ &= -\ddot{r}m + rm\dot{\theta}^2 + rm\dot{\phi}^2 \sin^2\theta + F_r^g + F_r^a \end{aligned} \tag{11}$$

Traction force is measured by a load cell of the ground segments, which provides information to a controller of the DC machine. The DC machine can then regulate the rate of the unwinding speed $\dot{r}$. Considering the traction force and the unwinding speed, the mechanical energy during the generation phase is shown as follows

$$E^{gen} = \int_0^{t_g} F^t \dot{r} dt \tag{12}$$

where t_g is the duration of the generation phase.

B. Glider in Recovery Phase

No traction force is applied to the glider in the recovery phase, and the glider can use its control surfaces to adjust its attitude. The external forces acting on the glider include the lift force L, drag force D, thrust T, and gravitational force mg. Then the equations of motion for the glider are expressed as. In addition, we also consider the wind effect on the glider [19]. As we assumed that wind is a function of altitude, therefore the time rate of wind velocity can be denoted as the following.

$$\dot{V}_{wx} = -\frac{\partial V_{wx}}{\partial h} V_e \sin\gamma \tag{13}$$

Then, the equations of motion with variable winds are formulated as below

$$
\begin{aligned}
\dot{x} &= V_e \cos\gamma \cos\psi + V_{wx} \\
\dot{y} &= V_e \cos\gamma \sin\psi \\
\dot{z} &= -V_e \sin\gamma \\
\dot{V_e} &= \frac{T\cos\alpha - D}{m} + g\sin\gamma + V_e \frac{\partial V_{wx}}{\partial h}\cos\psi \sin\gamma \cos\gamma \\
\dot{\gamma} &= -\frac{(T\sin\alpha + L)\cos\Phi}{mV_e} + \frac{g\cos\gamma}{V_e} - \frac{\partial V_{wx}}{\partial h}\cos\psi \sin^2\gamma \\
\dot{\psi} &= -\frac{(T\sin\alpha + L)\sin\Phi}{mV_e\cos\gamma} - \frac{\partial V_{wx}}{\partial h}\sin\psi \tan\gamma
\end{aligned}
\tag{14}
$$

where V_e is the effective speed of a glider, γ is the angle between the velocity and the horizontal plane, ψ is the heading angle, α is the angle of attack, Φ is the bank angle. The x-axis of the local coordinate $\boldsymbol{C}$ is aligned to the effective velocity. The transformation matrix between local coordinate $\boldsymbol{C}$ and inertial coordinate $\boldsymbol{E}$ is determined by

$$
\begin{aligned}
C_{CE} &= [C_1(\Phi)]\,[C_2(\gamma)]\,[C_3(\psi)] \\
&= \begin{bmatrix} \cos\gamma\cos\psi & \cos\gamma\sin\psi & -\sin\gamma \\ -\cos\Phi\sin\psi + \sin\Phi\sin\gamma\cos\psi & \cos\Phi\cos\psi + \sin\Phi\sin\gamma\sin\psi & \sin\Phi\cos\gamma \\ \sin\Phi\sin\psi + \cos\Phi\sin\gamma\cos\psi & -\sin\Phi\cos\psi + \cos\Phi\sin\gamma\sin\psi & \cos\Phi\cos\gamma \end{bmatrix}
\end{aligned}
\tag{15}
$$

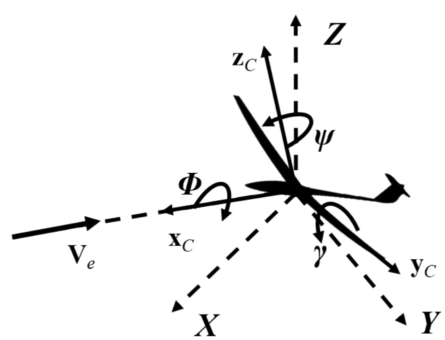

Fig. 5 Cartesian / local coordinates

C. Winch and DC Machine Model

The winch is designed and built for the interconnection between a DC machine and a glider. During the generation phase, this model converts the traction force to the rotational motion of the generator. For the recovery phase, the rotational motion from the motor rewinds the unwound cable to get prepared for the next energy generation phase. The dynamic model of the winch is formulated as

$$
I_{\mathrm{w}}\alpha_{\mathrm{w}} = r_{\mathrm{w}}F^t - M_{\mathrm{c}} - M_{\mathrm{gen}} \tag{16}
$$

where I_{w} is the moment of inertia of the winch, α_{w} is the angular acceleration of the winch, r_{w} is the winch radius, F_t is the traction force, M_{c} is the coulomb friction moment, and M_{gen} is the torque of the DC machine.

Considering the AWES has two operational phases, a generator and a motor are required to harvest energy in the generation phase and retrieve the glider back in the recovery phase. We utilize the integrated motor/generator technology that simultaneously adopts a permanent magnet DC machine working as a generator and motor. As shown in Fig. 6, an asymmetric half-bridge power converter is used to change the working modes.

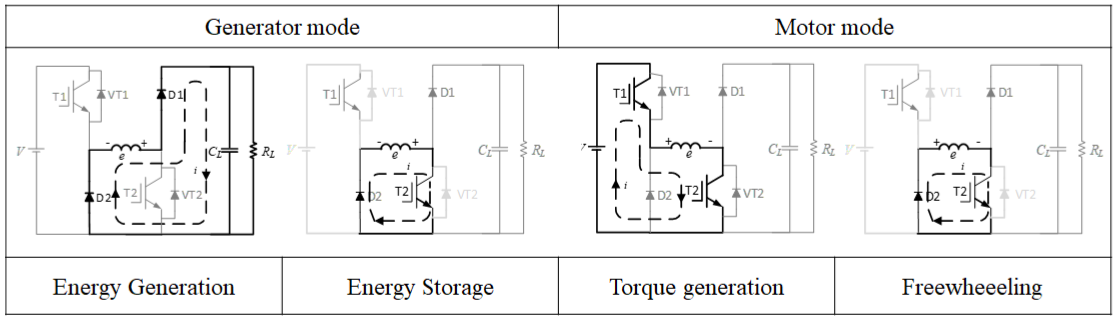

Fig. 6 Function of half-bridge

In the generation phase, the DC machine working under the generation mode has two stages, namely energy generation and energy storage, which is controlled by the switch T2, shown in Fig. 6. When the switch is turned off, the current flows through two diodes and is expressed as below

$$\begin{aligned} e &= u_L + Ri + L_a \frac{di}{dt} + 2U_d \\ i &= \frac{u_L}{R_L} + C_{\text{Link}} \frac{du_L}{dt} \end{aligned} \tag{17}$$

where e is the counter-electromotive force (CEMF) of the armature winding, u_L is the voltage of the load side, R is the armature resistance, L_a is the armature inductance, U_d is the voltage drop of the diode and switch, R_L is the load resistance, C_{Link} is the DC-link capacitor, and i is the armature current, which will also determine the electromagnetic torque T_e of the machine. The dynamic motion of the machine is governed by the kinematic equation, expressed as

$$\begin{aligned} T_e &= K_t i \\ J \frac{d\omega}{dt} &= T_e - T_L - B_m \omega - T_f \\ e &= K_e \omega \end{aligned} \tag{18}$$

where J is the moment of inertia of the rotor, T_L is the load torque from the glider, B_m is the viscous friction coefficient, T_f is the Coulomb friction torque, ω is the rotation speed of the machine, which also determines the CEMF, and K_e is the voltage constant of the machine. In addition, it should be noted that T_e and T_L have different signs in the generation mode and motor mode, which is determined by

$$\begin{aligned} &\text{if } T_e, T_L < 0 : \text{generator mode} \\ &\text{if } T_e, T_L > 0 : \text{motor mode} \end{aligned} \tag{19}$$

In contrast, when the switch T2 is turned on, the current flows through diode D2 to switch T2 and follows the voltage equation

$$e = Ri + L_a \frac{di}{dt} + 2U_d \tag{20}$$

In this case, the current will increase when the CEMF has the same direction as the armature current. It generally increases the power generation capability by increasing the electromagnetic torque. In this paper, considering we apply the glider's optimal trajectory to obtain the maximum energy generation, the converter in the generator mode will be a passive rectifier. The generator will only work on the energy generation stage to simplify the control strategy. However, we can also apply the maximum power point tracking algorithm on the generator side to improve the net energy generation.

In the recovery phase, the DC machine works in the motor mode and has two working stages, namely torque generation and freewheeling, as shown in Fig. 6, by controlling the switches T1 and T2. When both switches are turned on, the current flows through two switches and is governed by the armature voltage equation:

$$V_{dc} = e + Ri + L_a \frac{di}{dt} + 2U_d \tag{21}$$

where V_{dc} is the voltage of the DC power source. In contrast, when only switch T2 is turned on, the current cannot suddenly decrease to zero and will freewheel through diode D2. In this case, the current will decrease as the CEMF has the opposite direction with the armature current, which generally decreases the output torque. By using a proportional-integral (PI) controller, the duty cycle of the switch T1 can be controlled based on the feedback of motor speed to achieve constant speed control. A maximum power point tracking algorithm can also be applied to the motor to find a balance between energy consumption and retrieving time to achieve the maximum energy gain.

IV. Optimal Control Problem

In the generation phase, the glider flies like a kite and keeps pulling the tether line to generate the energy from the ground station. When the generation phase is over, the glider changes its wing shape to fly or dive to the initial point of the generation phase. Nonlinear programming is applied here to determine the optimized flight path and corresponding control commands for both phases. This optimal control problem can be considered as two separate problems associated with the generation and recovery phases. For the recovery phase, two different airborne platforms are used to determine which type of glider is more advantageous in terms of increasing energy efficiency in every cycle.

A. Generation Phase

During the generation phase, the accumulative energy term, $F^t \dot{r}$, is to be maximized. The direction of the traction force F^t is aligned with the tether line. Therefore, we need to extract the radial direction component of the acceleration of a glider in the spherical coordinate. The cost function is expressed as

$$J_G = \int_0^{t_g} F^t \dot{r}\, dt \tag{22}$$

where the traction force is determined from

$$F^t = -\ddot{r}m + rm\dot{\theta}^2 + rm\dot{\phi}^2 \sin^2\theta + F_r^g + F_r^a \tag{23}$$

The optimal control problem during the generation phase is formulated as

$$\begin{aligned}
&\max_{\Phi} && J_G && (24)\\
&\text{s.t.} && \dot{x}_g = f(x_g, u_g) && (25)\\
&\text{initial condition} && x(0) = x_0 && (26)\\
&\text{terminal condition} && r(t_g) = r_t && (27)\\
&\text{control variable} && \underline{\Phi} \le \Phi \le \overline{\Phi} && (28)\\
& && \dot{r} = \text{const} && (29)\\
& && \underline{\theta} \le \theta \le \overline{\theta} && (30)\\
& && \underline{\phi} \le \phi \le \overline{\phi} && (31)\\
& && L = \frac{1}{2}\rho S_u V_e^2 C_{L_g},\ D = \frac{1}{2}\rho S_u V_e^2 C_{D_g} && (32)\\
& && \frac{F_\theta}{m} = r\ddot{\theta} - r\dot{\phi}^2 \sin\theta\cos\theta + 2\dot{\theta}\dot{r} && (33)\\
& && \frac{F_\phi}{m} = r\ddot{\phi}\sin\theta + 2r\dot{\theta}\dot{\phi}\cos\theta + 2\dot{\theta}\dot{\phi}\sin\theta && (34)\\
& && \frac{F_r}{m} = \ddot{r} - r\dot{\theta}^2 - r\dot{\phi}^2\sin^2\theta && (35)
\end{aligned}$$

where $\{\theta, \phi, r, \dot{\theta}, \dot{\phi}\}$ are the states, the bank angle Φ is the control variable, and C_{L_g} and C_{D_g} are constant in this phase. During this phase, we assume that $\dot{r}$ is constant. Then the distance between the glider and the ground segment increases at a fixed rate. The aerodynamic forces are calculated based on the unfolded wing area S_u. $\underline{\Phi}$ and $\overline{\Phi}$ are the lower and upper bound of the bank angle input, $\underline{\theta}$ and $\overline{\theta}$ are the lower and upper bound of the zenith angle, and $\underline{\phi}$ and $\overline{\phi}$ are the lower and upper bound of the azimuth angle, respectively.

B. Recovery Phase

When the glider needs to be recovered, the glider flies back to the initial point of the generation phase. And the motor rewinds the tether line. In this phase, we need to minimize the energy consumption of both the glider and the DC machine. The glider changes to a folded configuration, which will contribute to reduced resistance and time. We assume that the motor operates with constant power. The objective function is written as

$$J_R = -\int_{t_g}^{t_f} P_{\text{rw}} dt - \int_{t_g}^{t_f} P(T) dt \tag{36}$$

where t_f is the duration of the entire cycle, P_{rw} is the power consumption of the ground motor, which is assumed to be constant, $P(T)$ is a function of the power consumption due to the thrust from a glider. For the folded wing configuration case, the aerodynamic parameters $(C_{L0f}, C_{L_\alpha f}, C_{D0f}, C_{D_\alpha 1f}, C_{D_\alpha 2f})$ and wing area S_f will be applied to calculate the aerodynamic forces. In this phase, the glider is not affected by the tether reaction force. The initial condition of this problem is the terminal condition of the generation phase problem. Then, we can formulate the optimal control problem of the folded wing configuration for the recovery phase, written as

$$\begin{aligned}
&\min_{T,\alpha,\Phi} && J_R && (37)\\
&\text{s.t.} && \dot{x}_r = f(x_r, u_r) && (38)\\
&\text{terminal condition} && x_r(t_f) = x_g(0) && (39)\\
&\text{control variable} && 0 \le T \le T_{\max}, \alpha_{\min} \le \alpha \le \alpha_{\max}, \underline{\Phi} \le \Phi \le \overline{\Phi} && (40)\\
& && C_{L_f} = C_{L0f} + C_{L_\alpha f}\alpha,\ C_{D_f} = C_{D0f} + C_{D_\alpha 1f}\alpha + C_{D_\alpha 2f}\alpha^2 && (41)\\
& && L = \frac{1}{2}\rho S_u V_e^2 C_{L_f},\ D = \frac{1}{2}\rho S_u V_e^2 C_{D_f} && (42)\\
& && \dot{x} = V_e \cos\gamma \cos\psi + V_{wx} && (43)\\
& && \dot{y} = V_e \cos\gamma \sin\psi && (44)\\
& && \dot{z} = -V_e \sin\gamma && (45)\\
& && \dot{V}_e = \frac{T\cos\alpha - D}{m} + g\sin\gamma + V_e \frac{\partial V_{wx}}{\partial h}\cos\psi \sin\gamma \cos\gamma && (46)\\
& && \dot{\gamma} = -\frac{(T\sin\alpha + L)\cos\Phi}{mV_e} + \frac{g\cos\gamma}{V_e} - \frac{\partial V_{wx}}{\partial h}\cos\psi \sin^2\gamma && (47)\\
& && \dot{\psi} = -\frac{(T\sin\alpha + L)\sin\Phi}{mV_e\cos\gamma} - \frac{\partial V_{wx}}{\partial h}\sin\psi \tan\gamma && (48)\\
& && P(T) = PT_0 + PT_1 \times T + PT_2 \times T^2 && (49)
\end{aligned}$$

where PT_0, PT_1, and PT_2 are the coefficients for the power consumption of the glider's motor. These parameters are extracted from experimental tests. In the recovery phase problem with unfolded wing configuration, different parameters of aerodynamic coefficients $(C_{L0u}, C_{L_\alpha u}, C_{D0u}, C_{D_\alpha 1u}, C_{D_\alpha 2u})$ and wing area S_u are used to determine the coefficients C_{L_u} and C_{D_u} and forces.

V. Simulation

A. Integrated Model

To build the entire structure of the AWES, we need to connect all subsystem models. In this paper, we utilize Matlab Simulink to validate the net energy gain of the production cycle. Figure 3 demonstrates the overall system and relations between the subsystems.

During the Generation phase, the glider has an unfolded wing configuration equivalent to the conventional glider geometry. It provides traction force to the winch. The winch converts the traction force to the generator's rotational motion. The glider changes to folded wing configuration for the recovery phase and flies back to the initial generation phase location while the motor is rewinding the tether line. The DC machine specifications are described in Table 1

Winch / DC machine specification	
radius $[m]$	0.03
mass [kg]	0.066
back-emf constant $[V/rpm]$	0.013
total inertia $\left[\text{kg} \cdot m^2\right]$	0.000192
viscous friction coefficient $[N \cdot m \cdot s]$	0.0002
coulomb friction torque $[N \cdot m]$	0.11337

Table 1 Specifications of a winch and DC machine

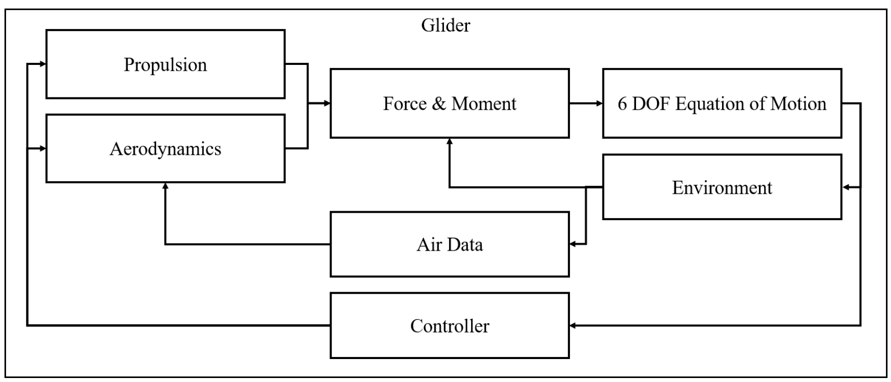

Fig. 7 The overview of a glider model

The glider model in the simulation environments consists of several blocks, as shown in Fig. 7. The equation of motion block is built based on the dynamics of the glider. The environment block generates gravitational force, air density, and wind speed, based on the location and velocity of the glider. Air Data block calculates airspeed, angle of attack, and dynamic pressure. The controller block follows the control input from nonlinear programming. The Aerodynamic block generates aerodynamic coefficients. Force & Moment block sums all the external forces and moments acting on the glider. The glider has two configurations with the main wing, as shown in Fig. 2. We choose an arbitrary wingspan ratio to fold. In Table. 2, the glider's specification for both configurations are shown as below

Glider Specification	Folded	Unfolded
Wingspan $[m]$	0.5	1.1
Wing area $\left[m^2\right]$	0.106	0.204
C_{L_0}	0.0833	0.1956
$C_{D_{\min}}$	0.0182	0.0051
$\frac{C_L}{C_D}_{\max}$	81.4	18.9
Length $[m]$	0.867	
Weight [kg]	0.738	

Table 2 Glider Specifications with unfold/fold configurations

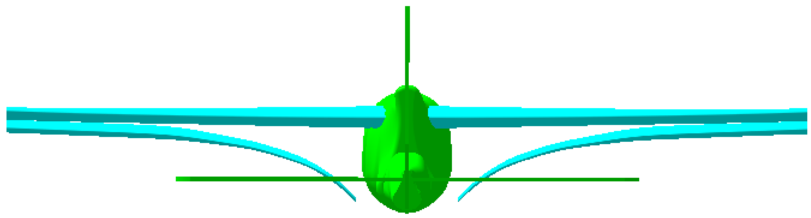

Fig. 8 Folded wing configuration

In order to extract the aerodynamic characteristics for two configurations, we used "XFLR5", one of the well known Computational Fluid Dynamics (CFD) tools, to extract coefficients under a varying angle of attack. In this analysis, the effect of the fuselage is not considered. The lift and drag coefficients are shown in Fig. 9. As a general glider, unfolded wing configuration has large $\frac{C_L}{C_D}$ than folded wing configuration. For the folded configuration, the slope of lift coefficient is larger, and the minimum drag is smaller than that from the folded wing configuration.

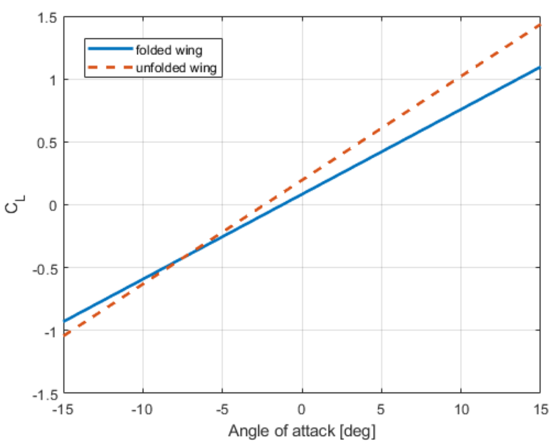

(a) Lift coefficients

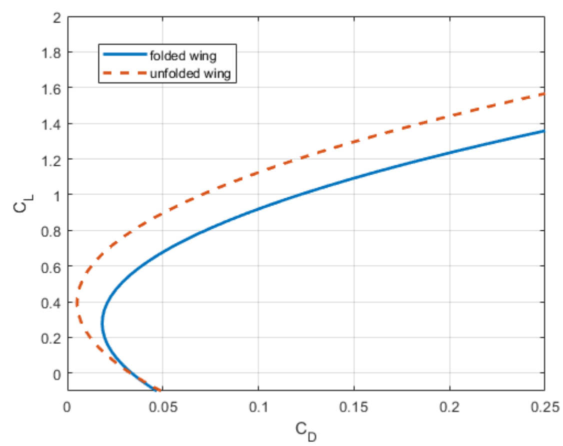

(b) Drag polar

Fig. 9 Aerodynamic coefficients

B. Optimal Trajectories

Combined with the two problems, the optimal path will be calculated, as shown in Fig. 10. The trajectory for the generation phase is designed for maximizing the energy harvested. On the other hand, the recovery trajectory is determined for minimizing energy consumption for both the airborne platform and ground DC machine. If the DC machine harvests energy, the sign of the energy is positive. The sign of energy is negative when the DC machine or glider consumes energy.

1. Generation Phase

The initial condition and the terminal condition and constraints of the generation phase are listed in Table 3. In the generation phase, the energy harvested by the glider is $879J$ in $30s$. Most of the time during the generation phase, the trajectory follows the "8" shape shown in Fig. 12. While the glider following the shape, the attitude angles, such as θ and ϕ, change periodically, shown in Fig.11a. The distance increases with a constant rate $\dot{r}$ till it reaches 15 m at the end of 30 seconds. In this phase, we set aerodynamic coefficients for C_{L_g} and C_{D_g} as 1.33 and 0.65 respectively.

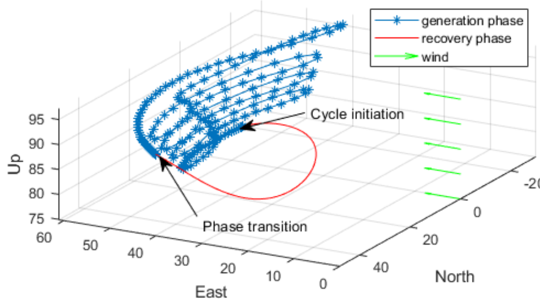

(a) Folded wing trajectory

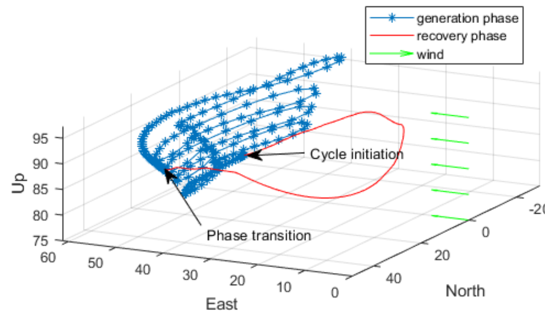

(b) Unfolded wing trajectory

Fig. 10 Trajectories of one cycle

States	Initial Condition	Terminal condition	Constraints
θ [rad]	0.52	-	$0.1 \leq \theta \leq 0.6$
ϕ [rad]	0	-	$-1 \leq \theta \leq 1$
r [m]	95	110	-
$\dot{\theta}$[rad/s]	0.18	-	-
$\dot{\phi}$[rad/s]	0.18	-	-
$\dot{r}$[m/s]	0.5	0.5	$\dot{r} = 0.5$

Table 3 States of the generation phase

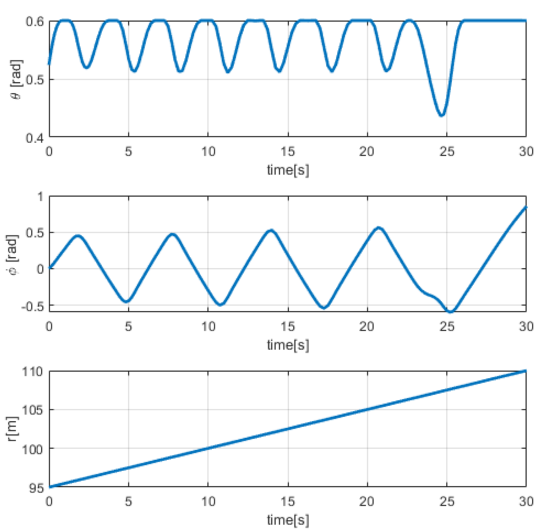

(a) History of the states

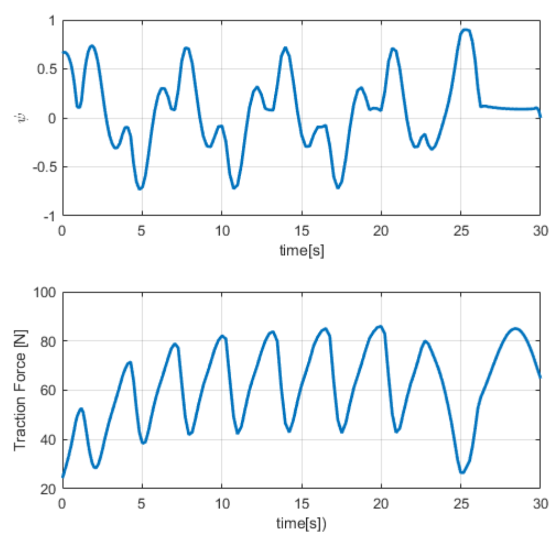

(b) Control input and traction force

Fig. 11 History of generation phase

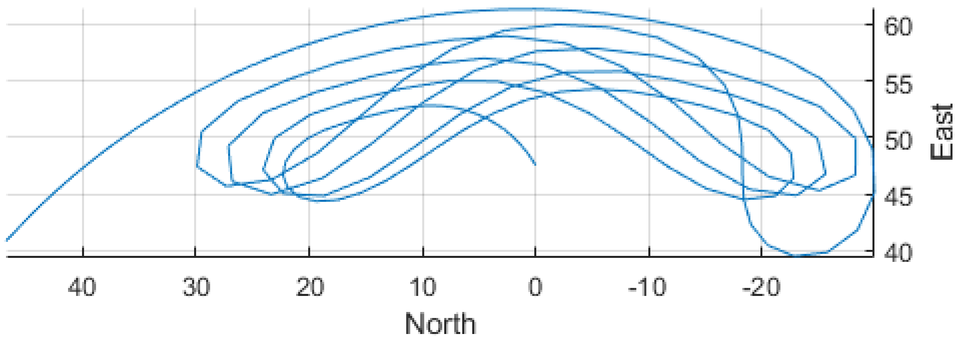

Fig. 12 Projected view of generation phase

2. Recovery Phase

In the recovery phase, the initial states are the same as the terminal states of the generation phase, as shown in Table 4. In the recovery phase, the glider flies back to the initial position of the generation phase, as shown in Fig. 13. Two configurations with different aerodynamic characteristics lead to different flight paths. In addition, the time histories of states are demonstrated in Fig. 14a. As shown in Fig. 14b, the power consumption of the ground motor for the unfolded wing significantly increases to rewind the tether line. Furthermore, the duration of the unfolded wing configuration is more extended than that of the folded wing configuration.

States	Initial Condition	Terminal condition	Constraints
x [m]	$r(t_g)\sin\theta(t_g)\cos\phi(t_g)$	$r(0)\sin\theta(0)\cos\phi(0)$	-
y [m]	$r(t_g)\sin\theta(t_g)\sin\phi(t_g)$	$r(0)\sin\theta(0)\sin\phi(0)$	-
z [m]	$r(t_g)\cos\theta(t_g)$	$r(0)\cos\theta(0)$	-
V_e[m/s]	$V_e(t_g)$	$V_e(0)$	$0 \leq V_e \leq 40$
γ[rad/s]	$\arcsin\frac{\mathbf{V}_{ez}(t_g)}{\lVert\mathbf{V}_e(t_g)\rVert}$	$\arcsin\frac{\mathbf{V}_{ez}(0)}{\lVert\mathbf{V}_e(0)\rVert}$	$-0.6 \leq \gamma \leq 0.8$
ψ[m/s]	$\arctan\frac{\mathbf{V}_{ey}(t_g)}{\mathbf{V}_{ex}(t_g)}$	$\arctan\frac{\mathbf{V}_{ey}(0)}{\mathbf{V}_{ex}(0)}$	-

Table 4 States of the recovery phase

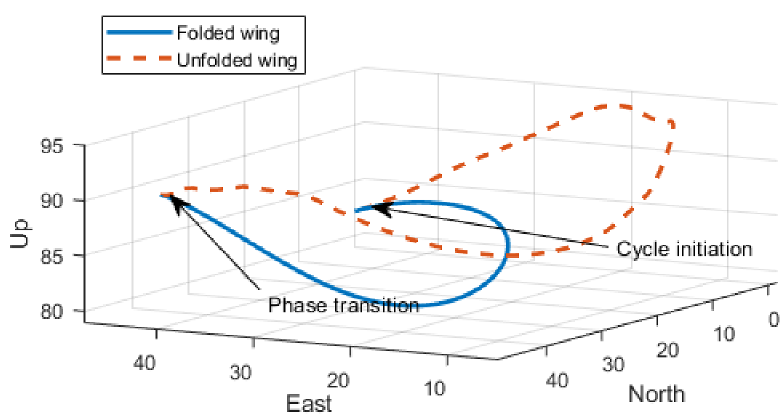

Fig. 13 Trajectories of recovery phase with two different configuration glider

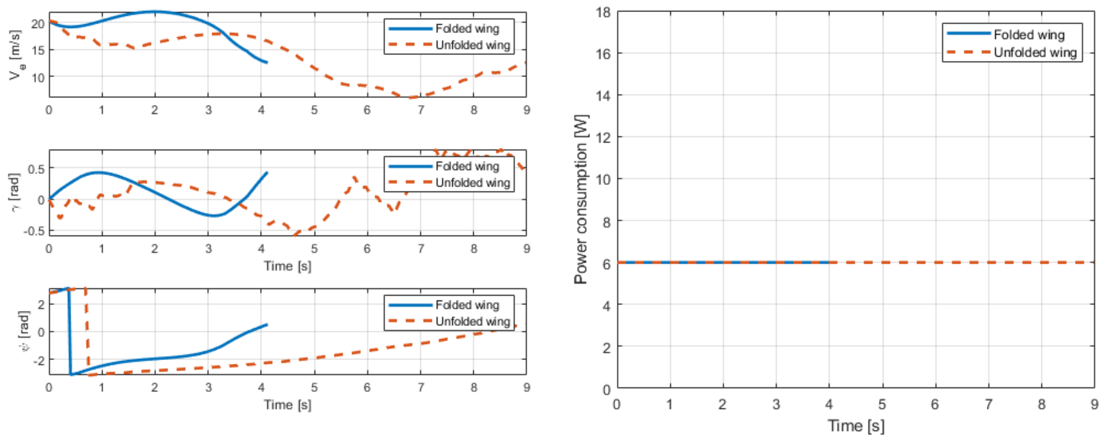

(a) History of the states **(b) Power consumption of two configurations**

Fig. 14 History of recovery phase

	Folded	Unfolded
Period [s]/(Rec. phase)	34.11 / (4.11)	38.97 / (8.97)
Net energy gain [J]/(Rec. phase)	854.28 / (-24.72)	825.13 / (-53.87)

Table 5 Result of two configurations from nonlinear programming

3. Nonlinear model simulation

In order to verify our results obtained from nonlinear programming, we simulate the formulated optimal control problem under the same assumed conditions using Simulink. As shown in Fig. 16, the simulation also demonstrates that a folded wing configuration shows improved net energy gain and reduced cycle duration compared to those for an unfolded wing configuration. The detailed results are shown in Table. 6.

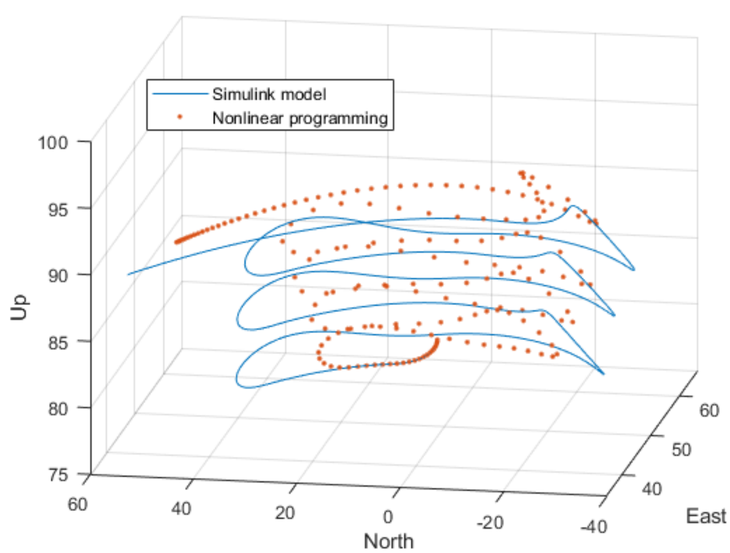

Fig. 15 Generation trajectories

Overall, the folded wing configuration is advantageous in terms of energy consumption and duration. The airborne

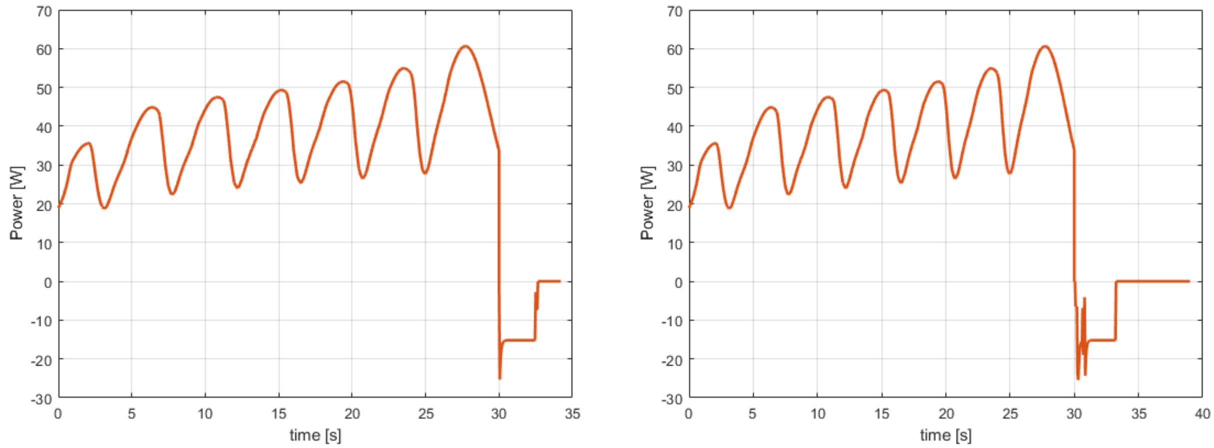

(a) Power history of folded wing configuration **(b) Power history of unfolded wing configuration**

Fig. 16 Power history over a cycle for two configurations

	Folded	Unfolded
Period [s]/(Rec. phase)	34.11 / (4.11)	38.97 / (8.97)
Net energy gain [J]/(Rec. phase)	1177.8 / (-39.00)	1129.3 / (-48.50)

Table 6 Result of two configurations from nonlinear model simulation

platform we consider is only a 1m-size RC glider. Based on the simulation, the folded configuration has reduced the time by 16%, and decreased the energy consumption by 24% for one cycle. It shows that if multiple cycles are considered, its advantages will be more significant. For example, 30 minutes of the operational period, the unfolded-wing glider can run 46 cycles and harvest $52kJ$. Instead, the folded option can run more than 52 cycles and generate $61kJ$.

VI. Conclusion

This paper demonstrates the new concept of the airborne wind energy system (AWES) with a foldable wing to improve energy and time efficiency. First, we build a glider and a DC machine to emulate their mechanical and electrical characteristics. We then formulate optimal control problems with different dynamics and constraints based on the multi-phase AWES operations. A folded wing, which contributes to reduced wind resistance during the recovery phase, leads to a reduction in power consumption. Comparative simulation is provided to verify that the new approach has enhanced energy and time efficiency. Future research will explore the operations of the physical AWES in outdoor environments.

References

[1] Statistics, G. W., "Global wind energy council," *Washington, DC, USA*, 2017.

[2] Loyd, M. L., "Crosswind kite power (for large-scale wind power production)," *Journal of energy*, Vol. 4, No. 3, 1980, pp. 106–111.

[3] Cherubini, A., Papini, A., Vertechy, R., and Fontana, M., "Airborne Wind Energy Systems: A review of the technologies," *Renewable and Sustainable Energy Reviews*, Vol. 51, 2015, pp. 1461–1476.

[4] Lunney, E., Ban, M., Duic, N., and Foley, A., "A state-of-the-art review and feasibility analysis of high altitude wind power in Northern Ireland," *Renewable and Sustainable Energy Reviews*, Vol. 68, 2017, pp. 899–911.

[5] Jehle, C., and Schmehl, R., "Applied tracking control for kite power systems," *Journal of Guidance, Control, and Dynamics*, Vol. 37, No. 4, 2014, pp. 1211–1222.

[6] Williams, P., Lansdorp, B., and Ockesl, W., "Optimal crosswind towing and power generation with tethered kites," *Journal of guidance, control, and dynamics*, Vol. 31, No. 1, 2008, pp. 81–93.

[7] Canale, M., Fagiano, L., and Milanese, M., "KiteGen: A revolution in wind energy generation," *Energy*, Vol. 34, No. 3, 2009, pp. 355–361.

[8] Bormann, A., Ranneberg, M., Kövesdi, P., Gebhardt, C., and Skutnik, S., "Development of a three-line ground-actuated airborne wind energy converter," *Airborne wind energy*, Springer, 2013, pp. 427–436.

[9] Fagiano, L., Zgraggen, A. U., Morari, M., and Khammash, M., "Automatic crosswind flight of tethered wings for airborne wind energy: Modeling, control design, and experimental results," *IEEE Transactions on Control Systems Technology*, Vol. 22, No. 4, 2013, pp. 1433–1447.

[10] Krenciszek, J., Akindeinde, S. O., Braun, H., Marcel, C., Okyere, E., and Argatov, I., "Mathematical modeling of the pumping kite wind generator: Optimization of the power output," *URL: http://www. win. tue. nl/casa/meetings/special/ecmi08/pumpingkite. pdf*, 2008.

[11] Terink, E., Breukels, J., Schmehl, R., and Ockels, W., "Flight dynamics and stability of a tethered inflatable kiteplane," *Journal of Aircraft*, Vol. 48, No. 2, 2011, pp. 503–513.

[12] Rautakorpi, P., "Mathematical modeling of kite generators," Master's thesis, 2013.

[13] Milutinović, M., Kranjčević, N., and Deur, J., "Multi-mass dynamic model of a variable-length tether used in a high altitude wind energy system," *Energy conversion and management*, Vol. 87, 2014, pp. 1141–1150.

[14] Williams, P., Lansdorp, B., and Ockels, W., "Modeling and control of a kite on a variable length flexible inelastic tether," *AIAA Modeling and Simulation Technologies Conference and Exhibit*, 2007, p. 6705.

[15] Li, H., Olinger, D. J., and Demetriou, M. A., "Attitude tracking control of a groundgen airborne wind energy system," *2016 American Control Conference (ACC)*, IEEE, 2016, pp. 4095–4100.

[16] Li, H., Olinger, D. J., and Demetriou, M. A., "Attitude tracking control of an airborne wind energy system," *Airborne Wind Energy*, Springer, 2018, pp. 215–239.

[17] Ruiterkamp, R., and Sieberling, S., "Description and preliminary test results of a six degrees of freedom rigid wing pumping system," *Airborne wind energy*, Springer, 2013, pp. 443–458.

[18] Canale, M., Fagiano, L., Ippolito, M., and Milanese, M., "Control of tethered airfoils for a new class of wind energy generator," *Proceedings of the 45th IEEE Conference on Decision and Control*, IEEE, 2006, pp. 4020–4026.

[19] Weitz, L. A., "Derivation of a point-mass aircraft model used for fast-time simulation," *MITRE Corporation*, 2015.